AIAA JOURNAL
Vol. 43, No. 3, March 2005

High-Frequency Oscillating-Hot-Wire Sensor for Near-Wall Diagnostics in Separated Flows

Yongxiang Li* and A. M. Naguib†
Michigan State University, East Lansing, Michigan 48824

A new high-frequency oscillating-hot-wire sensor for magnitude and direction measurements of the wall-shear stress in separated flows is presented. The stress direction is determined from the phase angle between the imposed and measured oscillation velocity, and the corresponding magnitude is obtained from the low-pass filtered signal of the sensor, after removal of the modulating influence of the oscillation. The sensor was used to conduct measurements downstream of an axisymmetric backward-facing step (BFS) at different streamwise locations ranging from 0.3 to 10 step heights downstream of the step. The results agreed qualitatively with existing one-point measurements, such as the mean/rms skin-friction distribution, forward flow probability, and power spectra, in planar BFS flows. However, some fundamental quantitative differences were found including a shorter reattachment length and a larger streamwise location for the peak rms wall-shear fluctuations. These differences were attributed to the axisymmetric nature of the present geometry, transverse curvature of the step, or differences in the measurement methods. Additionally, the power spectra of the fluctuating wall-shear stress revealed the existence of two characteristic frequencies: $f^* = 0.1$ and 0.65. The former is associated with low-frequency shear-layer flapping, and the latter corresponds to the passage of the separated shear-layer vortex structures.

I. Introduction

THE importance of separating and reattaching flows in practical aerodynamic applications and research of fundamental fluid mechanics is well known. These flows have been extensively studied using various experimental and numerical techniques during the past decades. However, there is little information available in the literature on the turbulent wall-shear-stress field beneath separated flows. In this paper, a high-frequency oscillating-hot-wire (OHW) sensor is developed for use in time-resolved measurements of the wall-shear stress in such flows. The operation of the sensor is demonstrated in the flow past an axisymmetric bacward-facing step (BFS). A review of the pertinent literature on mean and fluctuating wall-shear measurements in BFS flows follows.

Westphal et al.[1] measured mean and rms skin-friction coefficients in a BFS flow using a wall pulsed wire. Devenport and Sutton[2] investigated an axisymmetric sudden expansion also using a wall pulsed wire. Later, Jovic and Driver[3] studied the effect of Reynolds number on the mean skin-friction coefficient in a BFS flow using a laser oil flow interferometry (LOI). Most recently, Spazzini et al.[4] measured the wall shear to investigate the flapping motion in a BFS flow using a special wall-mounted double hot-wire probe, whereas Tihon et al.[5] investigated wall-shear vectors behind a BFS using a three-segment electrodiffusion probe in a water channel.

Among the different approaches employed in the preceding studies, LOI is the most accurate wall-shear measurement technique known today, but it can only provide mean-shear measurements. An excellent review of this technique can be found in the paper by Naughton and Sheplak.[6] The rest of the methods infer the shear stress from heat/mass transfer from the sensor and require calibration. Most of the studies utilizing these methods obtained only mean and rms wall-shear information. Because the near-wall flow behind a backward-facing step is highly turbulent and flow reversal occurs frequently, it is difficult to conduct measurements of the wall-shear stress in this region. Fernholz et al.[7] did a comprehensive review of techniques for measurement of the wall-shear stress in wall-bounded and separated flows. They concluded that only wall hot wires and pulsed wires were capable of measuring the unsteady wall shear. But wall hot wires cannot be used in cases involving flow reversal. Wall pulsed wires, on the other hand, measure the wall-shear magnitude and direction, but their frequency response is limited to tens of hertz.

Although the measurements of Spazzini et al.[4] and Tihon et al.[5] are time resolved, the sensor of Spazzini et al.[4] is fundamentally based on thermal wake detection like pulsed anemometry, and the electrodiffusion probe of Tihon et al.[5] is based on mass-transfer effects and cannot be used for measurement in airflows.

Recently, Li and Naguib[8] demonstrated the use of an OHW sensor to remedy the "direction blindness" of single hot-wire probes. The concept of this new sensor was verified via comparison with laser-Doppler-velocimetery data in an unsteady pipe flow. Li and Naguib[8] showed that for accurate measurements, the velocity-frequency product $U_0 f_0$ (where U_0 is the oscillation velocity amplitude and f_0 is the oscillation frequency) must be larger than twice $u_f f_f$ (where u_f and f_f are characteristic velocity and frequency, respectively, of the flow unsteadiness). Furthermore, f_0 must be at least twice f_f to prevent aliasing in the recorded time series if time-resolved data are desired.

The prototype sensor used by Li and Naguib[8] was oscillated at a frequency of 490 Hz and U_0 of 0.5 m/s using a 63.5-mm long × 31.8-mm wide × 0.58-mm thick piezoelectric cantilever oscillator. This yielded a $U_0 f_0$ product that was more than five times larger than $u_f f_f$ of the unsteady pipe flow, which had a characteristic frequency of 15 Hz and flow velocity amplitude of 3 m/s.

The prototypical sensor used by Li and Naguib[8] is suitable for use in flows containing unsteady frequencies of the order of tens of hertz. However, many low-speed separated flow experiments that are established in the laboratory, for example, over an airfoil, backward facing step, bluff body, etc., involve significant flow unsteadiness occurring at frequencies of the order of hundreds of hertz to a few kilohertz. Therefore, OHW sensors with larger oscillation frequency are desired for diagnostics in these flows.

The current study is focused on the following: 1) the realization and characterization of OHW sensors that are capable of oscillating at frequencies of a few kilohertz (the construction of the sensors

Presented as Paper 2004-1041 at the AIAA 42nd Aerospace Sciences Meeting, Reno, NV, 5–8 January 2004; received 12 February 2004; accepted for publication 24 April 2004.

*Graduate Student, Department of Mechanical Engineering. Member AIAA.

†Associate Professor, Department of Mechanical Engineering. Senior Member AIAA.

is based on the use of small-size piezoelectric cantilever oscillators) and 2) demonstration of the operation of the new sensors to measure the wall-shear stress in an axisymmetric BFS flow.

II. Experimental Setup

A. Sensor Details

The operation of the OHW sensor is based on taking two very fast measurements (referred to as forward and backward measurements) from the hot-wire sensor at the center of oscillation: when it is moving with and against the flow. If the oscillation period is sufficiently small (i.e., the oscillation frequency is sufficiently high) for any substantial change to happen in the flow, it is possible to discern the direction of the flow from comparison of the two measurements during one oscillation cycle. The resulting OHW output is essentially an amplitude-modulated version of the classical hot-wire sensor output. To extract the magnitude of the velocity, the amplitude modulation is removed via low-pass filtering, and the resulting voltage is converted to velocity using the sensor's static calibration. On the other hand, the flow direction is obtained from the phase of the sinusoidal modulation of the signal. In particular, the phase difference between the wire output and the piezodriving voltage at the oscillation frequency experiences an 180-deg jump when the flow switches direction. Thus, the difference between the forward and backward measurements will be either positive or negative depending on the flow direction. Because a full oscillation cycle must be completed before the direction is determined, the sampling frequency of the velocity time series is equal to f_0.

Figure 1 shows a schematic drawing of the OHW sensor used in the current study. The sensor is mounted in a 7.62-mm-wide wall plug with a curved top surface with a radius of 50.8 mm to match the curvature of the outer shell behind the step of the test model. The prongs of the hot wire are attached using epoxy on one end of a 12.7-mm-long × 6.35-mm-wide × 0.58-mm-thick piezoelectric beam, protruding through 0.51-mm-diam holes in a Plexiglas® insert in the wall plug. At the opposite end to the prongs, the piezoelectric beam is rigidly fixed using a clamp made out of phenolic to electrically isolate the piezoelement's electrodes. In turn, the clamp is supported on two dowel pins that are force fitted to the wall-plug body. The pins provide rigid support to the piezoelement in the direction of oscillation while allowing the element's position to be adjusted in the wall-normal direction to place the hot wire at heights y_w up to 5 mm above the wall. Once at the desired location, two set screws are used to fix the sensor's position. For the results reported here, y_w is set to 97 μm (see Sec. III.D for more details), which was determined by viewing the hot wire in a plan normal to the wall-plug face under a microscope.

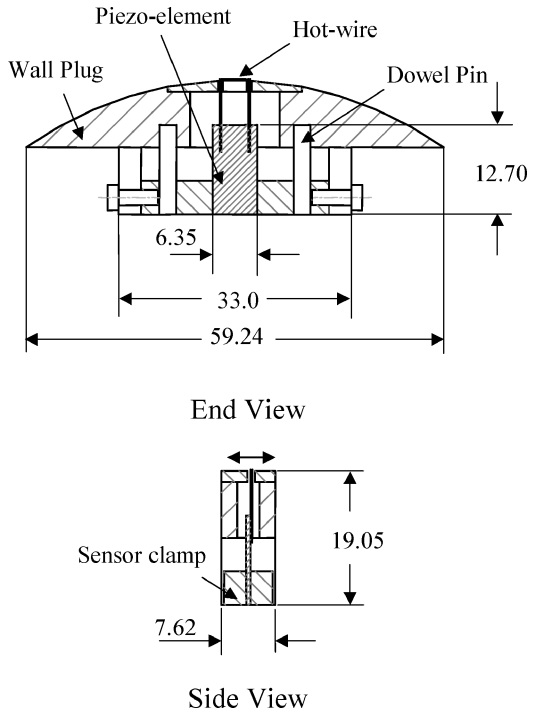

Fig. 1 Drawing of the sensor plug (dimensions in millimeters).

A 60-V peak-to-peak sinusoidal voltage was used to oscillate the hot wire at frequencies up to 4.8 kHz and displacement amplitude in the range 1–12 μm (about 0.25–3.25 wire diameters) with the highest amplitude corresponding to the piezoelement's resonant frequency of approximately 2 kHz. For measurements in the BFS flow, an oscillation frequency of 2.8 kHz was selected. The 2.8-kHz sensor is capable of time-resolved measurements in flows that have bandwidths extending to 1.4 kHz: an order of magnitude increased capability over the early prototype.

B. Calibration Facility

Although typical hot-wire sensors are known to have wide bandwidth of 20–40 kHz, evidence of substantial reduction in the dynamic response of hot wires near zero mean-flow velocity exists in the literature.[9] Therefore, with the use of kilohertz OHW, it is important to calibrate and check the hot-wire ability to respond to the imposed oscillation in a controlled environment where the mean velocity could be adjusted to very small value and the direction of the flow could be reversed. To this end, a Couette flow facility is used for calibration and characterization of the sensor response.

Figure 2 displays a cross-section view of the facility. It consists of a rotating disk with a diameter of 0.317 m that is placed parallel to but away from a stationary disk. For the current measurements, the rotating disk is made to spin at speeds up to 1900 rpm using a dc motor, and the spacing between the two disks is set to 0.6 mm using feeler gauges. The resulting velocity field between the two disks is that of a Couette flow, yielding a linear velocity profile with distance normal to the stationary plate. Thus, it is possible to mount wall sensors in the stationary plate and calibrate them against the mean shear stress (known from the rotational speed of the disk, the gap size, and the radius from the center of rotation to the location of the sensor) or mean velocity (which can be deduced from the mean shear stress and y_w). The accuracy of this type of calibration facility in establishing a Couette flow has been verified using direct numerical simulation by Khoo et al.[10] Using the results of their simulation in conjunction with the specific probe location and dimensions of the facility used here, the following was verified:

1) The flow velocity in the rotational (azimuthal) direction of the disk does vary linearly across the space between the two disks.

2) The radial flow velocity is less than 10% of the azimuthal velocity. (Because the radial velocity is directed parallel to the wire axis, its effect on cooling of the wire is an order of magnitude less

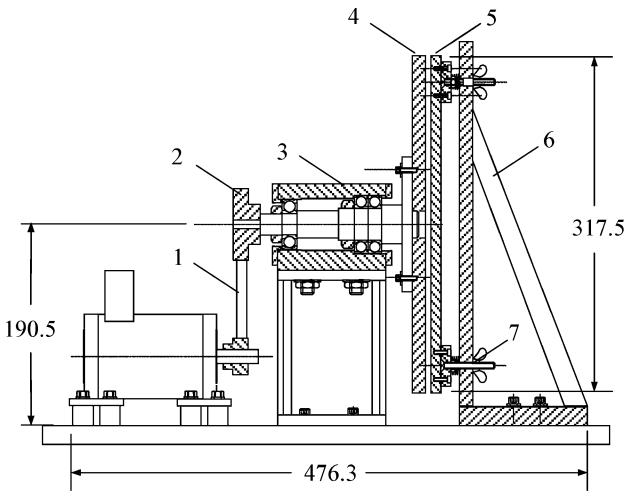

Fig. 2 Couette flow calibration facility: 1, timing belt; 2, timing pulley; 3, bearing assembly; 4, rotating disk; 5, stationary disk; 6, supporting bracket; and 7, spring-loaded support screw (dimensions in millimeters).

than the azimuthal velocity; thus, the calibration error caused by the nonzero radial velocity should be less than 1%.)

3) The wall-normal velocity is less than 0.01% of the azimuthal velocity, and hence its influence on the calibration could be ignored all together. Finally, it should be added here that Koo et al.[10] also calibrated near-wall hot wires successfully in the same type of Couette-flow facility and verified their operation in fully developed laminar and turbulent channel flow.

C. Axisymmetric Backward-Facing-Step Model

The axisymmetric BFS model is mainly composed of two aluminum tubings: upstream of the step, the tubing is 127.0 mm in diameter and 1.213 m in length, with an aluminum half-spherical nose made with a radius of 63.5 mm fitted at its upstream end; downstream of the step, the aluminum tubing with 101.6 mm outside diameter extends about 900 mm. The difference between the tubing diameters creates a nominal step height H of 12.7 mm. Finally, the downstream end of the model is terminated with conical tail section to avoid abrupt termination of the geometry.

The BFS model is placed at the center of a low-speed open-circuit wind tunnel. The test section is 1.829 m long, with a cross-sectional flow area of 610×610 mm^2. The freestream turbulence intensity in the test section was found to be less than 0.45% from measurements in the velocity range of 5–15 m/s.

Boundary-layer mean-velocity profiles were obtained at 0.5 mm upstream of the step using a single hot-wire probe. The boundary layer is tripped using sandpaper just downstream of the nose section and develops to two-dimensional (axisymmetric) turbulent boundary-layer state at the separation point. The Reynolds number based on boundary-layer momentum thickness is 1139, 2057, and 2739 for three freestream velocities: 5, 10, and 15 m/s, respectively.

The measurements on the model were taken primarily in the region extending from the step to 127.0 mm (i.e., 10 step heights) farther downstream. Figure 3 shows a magnified view of the measurement region. Within this zone, four sensor covers are located at the top, bottom, left, and right of the cylindrical model surface. There are static-pressure taps in sensor covers numbered 2, 3, and 4 in Fig. 3. The slot for sensor cover 1 could be used to install an oscillating-hot-wire sensor for wall-shear measurements or static-pressure taps mirroring those in cover 3. The static-pressure taps were primarily used to verify the alignment of the model parallel to the freestream direction.

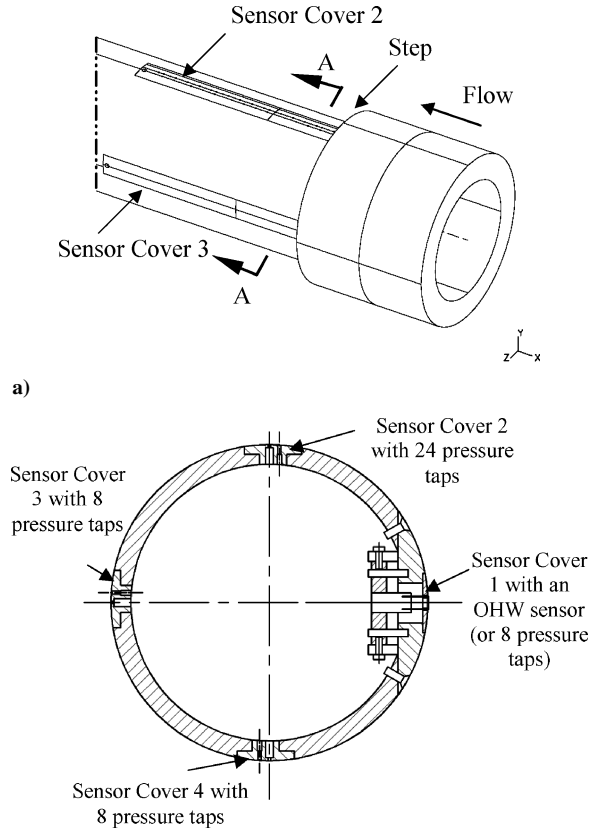

Fig. 3 Magnified view of the measurement zone showing wall-sensor covers: a) three-dimensional and b) cross-section view.

III. OHW Sensor Characteristics

A. OHW Magnitude Calibration

Figure 4 shows the hot-wire calibration obtained without wire oscillation (solid line), compared to that obtained from the mean hot-wire voltage for wire oscillation frequencies of 1.1, 2, 3, and 4 kHz. The no-oscillation calibration (referred to as STAT in the legend) extends down to a velocity of 0.1 m/s. On the other hand, data obtained during oscillation are shown for a velocity range that is larger than 0.3 m/s. In this range, a good agreement is evident between the results with/without the oscillation. This verifies that the high-frequency oscillation of the wire does not result in an anomalous or nonlinear behavior that can affect the wire's calibration or its accuracy in retrieving the velocity magnitude.

At mean-flow velocities that are less than U_0, rectification of the hot-wire output starts occurring with full rectification taking place at zero velocity. (No data are shown in Fig. 4 for this velocity range.) This nonlinear effect results in the mean hot-wire voltage during oscillation exceeding that without oscillation with the maximum error being $0.64U_0$ (mean value of a fully rectified sine wave with amplitude U_0) at zero flow velocity. However, as will be shown in Sec. III.C, near zero mean velocity the frequency response of the hot wire is sufficiently attenuated so that it cannot respond to the rectification frequency (twice f_0, or 5.6 kHz here). This was verified by inspecting the wire output voltage on the oscilloscope during oscillation in the absence of any flow. No rectification of the wire output was observed, and therefore this rectification error had no effect on the results. Notwithstanding the attenuation of the wire frequency response near zero mean velocity, which would affect the

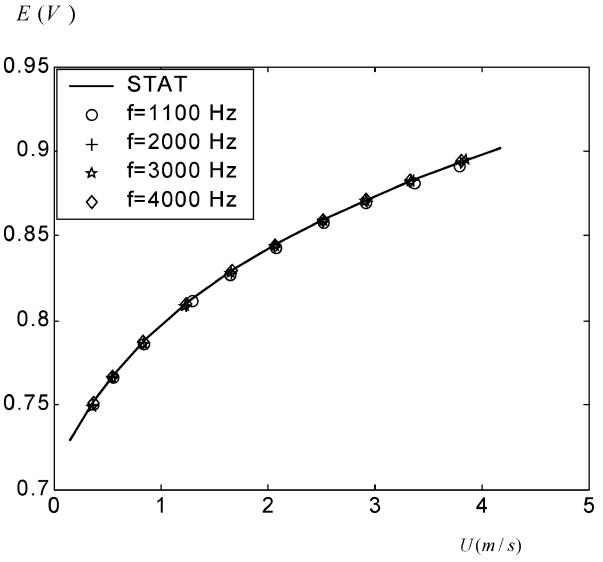

Fig. 4 Calibration of the hot wire with/without oscillation.

measurements only in the immediate vicinity of points of separation/reattachment, the bandwidth of the sensor was sufficient for resolving fluctuations of up to approximately 1 kHz near reattachment and 2 kHz or more at other points. This is more than sufficient for the current application, where most of the fluctuations are contained below 1 kHz, with the most energetic contribution centered around 160 Hz. The wire bandwidth at different mean velocities was determined in the Couette flow facility by oscillating the wire at different frequencies in the range 800 Hz–5 kHz while maintaining a certain mean velocity (or shear stress). A sample of those results at 2 kHz will be discussed in Sec. III.C.

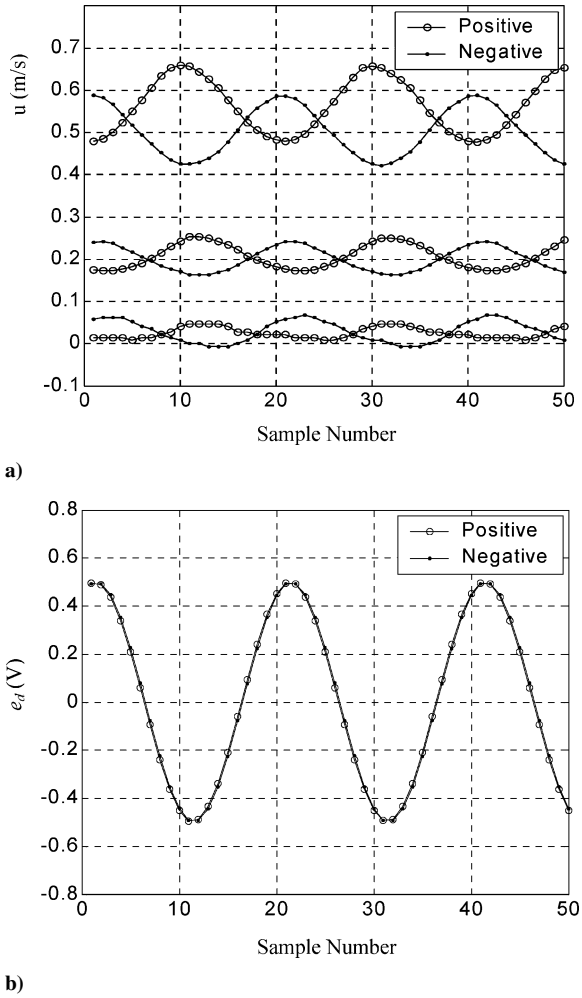

Fig. 5 Demonstration of the effect of the flow direction on the phase of the OHW modulation signal: a) OHW output and b) OHW driving signal.

B. Demonstration of OHW Direction Response

Flow-direction measurement by OHW sensors is based on the fact that the phase difference between the wire output and the piezodriving voltage, hereafter denoted by ϕ_{ohw}, at the oscillation frequency experiences an 180-deg jump when the flow switches direction. To demonstrate the concept, the OHW sensor was used to take measurements at different velocities under clockwise as well as counterclockwise rotation of the rotating disk in the Couette flow facility. The results are plotted in Fig. 5a for the velocities of $U = 0.03$, 0.2, and 0.55 m/s. For each speed, two data sets are plotted (open circles and dots) representing two opposing flow directions. For orientation purposes, Fig. 5b contains a plot of the driving voltage of the OHW. The data clearly demonstrate the reversal of phase of the wire sinusoidal modulation signal as the flow changes direction for all flow speeds. For the lowest flow velocity and negative direction, small (about 0.01 m/s) negative values of the sensor output are seen in Fig. 5a. Because this is the "raw" output of the sensor before demodulation and extraction of direction information, no negative values should be observed. The discrepancy is of the order of the accuracy of the calibration process in the vicinity of zero velocity.

C. Wire Dynamic Response to Imposed Oscillations

To examine how the wire responds to the imposed oscillations at different frequencies and flow velocities, the mean-removed hot-wire output was acquired and phase averaged with respect to the OHW driving voltage. The phase average aids in removing the effect of any background disturbances related to motor vibration influences

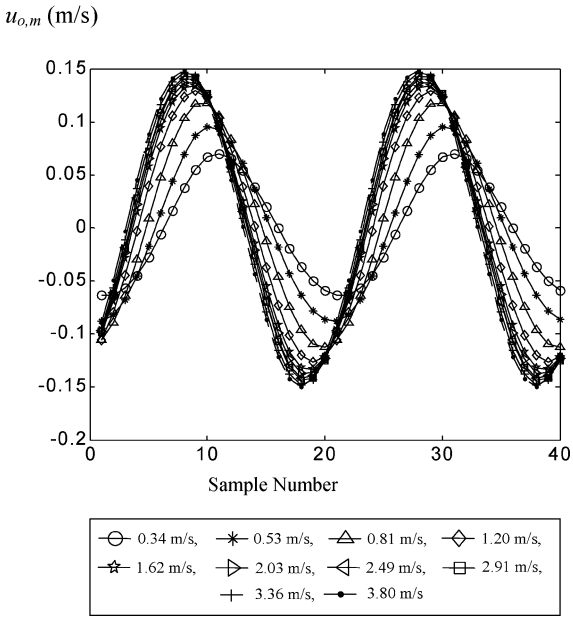

Fig. 6 Phase-averaged OHW velocity at oscillation frequency of 2 kHz for different mean velocities.

or other sources of noise. A portion of the resulting signal is shown in Fig. 6 for an oscillation frequency of 2 kHz and different mean velocities in the range 0.34–3.8 m/s. The reduced dynamic-response ability of the wire with decreasing speed is evident from the data as the amplitude of the measured oscillation velocity $u_{0,m}$ is attenuated, and an increased phase lag is observed with the reduction in the mean flow velocity.

For flow speeds larger than 1 m/s, $u_{0,m}$ is fairly constant. However, when the flow velocity drops below 1 m/s, larger attenuation is found. The reduction close to zero flow velocity is presumably caused by shifting of the primary heat-transfer mode of the wire from forced to natural convection, leading to a larger thermal time constant. Although the constant-temperature-anemometer (CTA) circuit compensates for the sensor's thermal response, the compensation generally works well for flow velocities larger than roughly 1 m/s where the thermal time constant apparently does not vary significantly. Below 1 m/s there seems to be appreciable change in the time constant, for which the CTA does not adapt. Additionally, at those low speeds the fraction of the heat transfer caused by conduction to the probe prongs becomes larger, contributing further to the reduced frequency response.

The reduction in the dynamic response should not cause a problem in operating the OHW sensors as long as the amplitude attenuation is not too large for the sinusoidal modulation of the wire output to be detectable at very low velocities. In Fig. 5a, the modulation signal at the oscillation frequency is detectable at flow velocities as low as 0.03 m/s.

In addition to amplitude attenuation, as the flow velocity decreases, a phase-angle delay is observed between the imposed and measured oscillation. The delay becomes progressively larger with decreasing flow velocity. In Fig. 6, the biggest phase lag is less than 90 deg, which is found at the lowest flow speed. Because this lag does not exceed 90 deg, it does not create a problem in direction determination, as explained in the following paragraph.

An example of a direction calibration for a wall-shear OHW sensor is shown in Fig. 7. For reference, the ideal ϕ_{ohw} response, exhibiting 180-deg phase jump with flow reversal, is also illustrated in the figure using a broken line. The deviation between the ideal and actual ϕ_{ohw} behavior is primarily caused by the limitation of the wire dynamic response near zero velocity, as just discussed. However, it is clear that notwithstanding this deviation, ϕ_{ohw} values in the positive-shear direction do not overlap with those in the negative-shear direction, showing that the shear direction can still be determined without ambiguity.

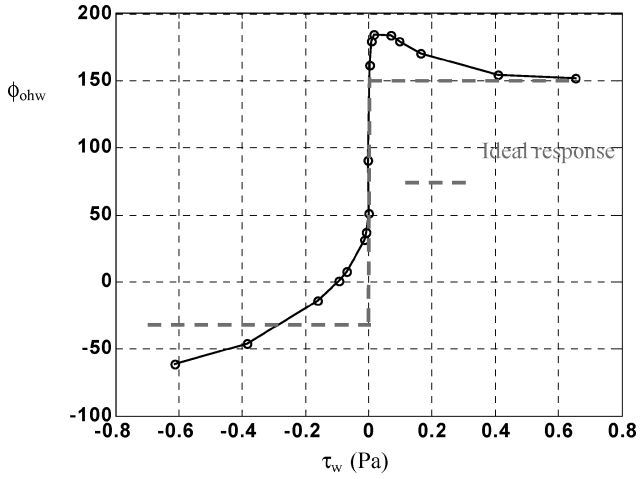

Fig. 7 Typical direction calibration of the OHW sensor.

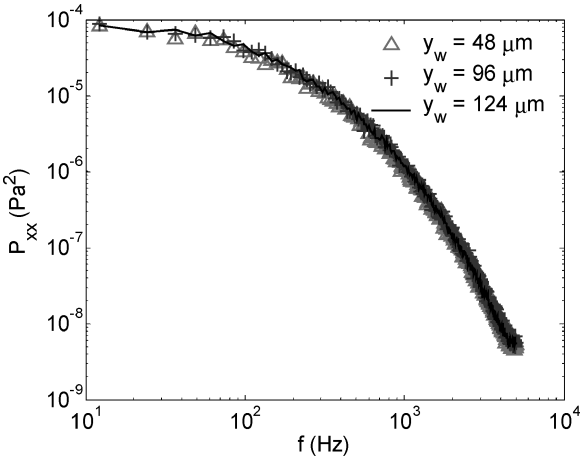

Fig. 8 Power spectra for wire heights of $y_w = 48$, 96, and 124 μm.

D. Effect of Wire Height Above the Wall

For a wall hot-wire sensor to measure wall-shear stress, the wire must be located within the viscous sublayer, that is, $y^+ < 5$ (or $y_w < 5\nu/u_\tau$), where $y^+ = y_w u_\tau/\nu$ is the wire height above the wall in viscous units, $u_\tau = \sqrt{\tau_w/\rho}$ is the friction velocity, ν is the fluid kinematic viscosity, ρ is the fluid density, and τ_w is the wall-shear stress. To experimentally check proper positioning of the wire above the wall, measurements were conducted with the height of the sensor set to three different values: 48, 96, and 124 μm. The streamwise location downstream of the step for the measurements ($x = 9.82H$) was chosen to be well downstream of the expected mean reattachment position x_r such that τ_w has recovered near its largest value after reattachment. The freestream velocity was set to 15 m/s, corresponding to Reynolds number based on step height of $Re_H = 13 \times 10^3$. No wire oscillation was imposed during this set of experiments because the measurement location is well downstream of the expected reattachment position, and hence there is no directional ambiguity of the flow. The work of Spazzini et al.[4] and Tihon et al.[5] provide supporting evidence that the flow at the chosen measurement location is always in the downstream direction. More importantly, the flow-direction-probability results from the current study, given later in Sec. IV. B, verify that the flow is in fact always in the downstream direction at $x = 9.82H$.

Figures 8 and 9 display the power spectra P_{xx} and normalized histograms, respectively, for data acquired at the three different wire heights. The data corresponding to the three different cases collapse well in both plots. The mean values of the wall-shear stress calculated from the histograms are 0.282, 0.276, and 0.275 Pa. The small variation of the measurements with the wire height indicates that all three positions are within the viscous sublayer, where the

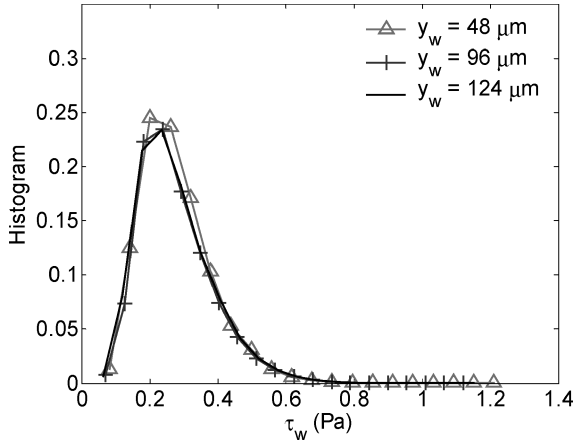

Fig. 9 Histogram for wire heights of $y_w = 48$, 96, and 124 μm.

velocity is linearly proportional to the wall shear stress. In fact, if the highest observed τ_w value of 0.282 Pa is used one viscous unit will be 31.3 μm. The corresponding wire heights are $y^+ = 1.5$, 3.1, and 4.0, that is, all positions are within the viscous sublayer. Based on this, the wire height was set to 97 μm for BFS measurements conducted here.

E. Effect of Wire Oscillation on the Flow

Although highly unlikely, it seemed appropriate to check whether the oscillation of OHW sensors disturbs the unsteady direction-reversing flow downstream of the backstep. For this purpose, data obtained at $Re_H = 13 \times 10^3$ and $x/x_r = 0.06$, 0.92, and 1.54, that is, before, close to, and after the mean reattachment point, were utilized. At each location, measurements were conducted when the oscillation was on as well as off. The former case corresponded to an OHW sensor with the oscillation frequency of 2.8 kHz, and the latter represented a conventional hot-wire sensor. The premise of the test is based on the fact that notwithstanding its directional blindness the conventional hot-wire output voltage should provide the correct magnitude of the wall-shear stress. Therefore, the low-pass-filtered voltage signal of the OHW, which also provides the magnitude information of the wall shear, should yield the same voltage output magnitude as the conventional hot wire. If the OHW operation does disturb the flow, then one would expect that the frequency spectrum, or some other statistical measure, of the low-pass-filtered OHW voltage would deviate from that obtained with the stationary wire.

Figure 10 shows a comparison between the power spectra of the raw voltage data of the oscillating- and conventional-hot-wire sensors at $x/x_r = 0.92$, labeled as SHW and OHW in the legend. A low-pass filter with a cutoff frequency of 1.4 kHz, or half of the oscillation frequency, was also applied to the OHW signal. Because the sampling frequency of the OHW sensor is also the oscillation frequency, this filtering eliminates any possible aliasing in the OHW signal. The spectra obtained from the filtered signal are also included in the plots in Fig. 10a. Inspection of the figure clearly shows that within the pass band of the filtered signal the voltage spectrum of the OHW and SHW sensors agree quite well. The imposed oscillation on the OHW sensor is also evident from the harmonic peak at $f = 2.8$ kHz. Therefore, one can conclude that the oscillating-hot-wire operation does not generate any flow anomaly. The energy level of the oscillation signal is at least two orders of magnitude larger than that of the flow at the oscillation frequency. This yields a strong signal-to-noise ratio, which is necessary for successful determination of the flow direction.

Another important observation in Fig. 10a is that the flow energy contained in frequencies above 1 kHz is only very small component of the total energy. This can be seen from the fact that the spectrum level at frequencies higher than 1 kHz is two orders of magnitude or more lower than the spectral peak value. Hence, the selected oscillation frequency should be high enough to resolve the wall-shear signature of the most energetic flow structures.

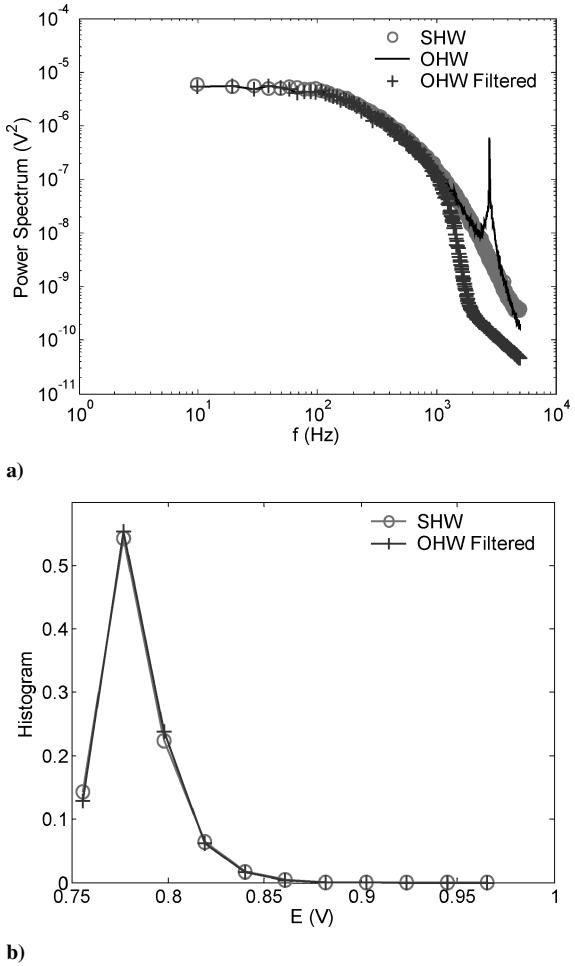

Fig. 10 Comparison of conventional- and oscillating-hot-wire data at $x/x_r = 0.92$: a) power spectra and b) histogram.

Further comparison between the oscillating and stationary hot-wire measurements was conducted by comparing the normalized histogram of the voltage magnitude obtained in both cases. As evident in Fig. 10b, OHW filtered and SHW histograms are similar. This suggests that the two measurement methods produce the same statistics of the voltage and hence, shear-stress, magnitude.

The data obtained at $x/x_r = 0.06$ and 1.54 are similar to those at $x/x_r = 0.92$, and so they are not shown here. Collectively, the results verify that the wire oscillation does not disturb the flow.

IV. One-Point-Measurement Results in the BFS Flow

A. Mean Reattachment Length

An OHW sensor as shown in Fig. 1 was used to measure τ_w at different streamwise locations extending from $x = 0.30H$ to $9.84H$. At the mean reattachment location x_r, the mean wall-shear stress equals zero. Thus, the streamwise distribution of the mean skin-friction coefficient C_f could be used to directly find x_r. Figure 11 is obtained for three Reynolds numbers based on step height of 4.3×10^3, 8.7×10^3, and 13×10^3. The vertical axis represents the mean skin-friction coefficient, and the horizontal axis indicates the corresponding normalized x location. The data for all Reynolds numbers have the same trend except at the first, most upstream, point. At $Re_H = 4.3 \times 10^3$, the mean skin-friction coefficient at this point is less than zero, whereas it is greater than zero for the other two.

Inspection of the wall-shear direction deduced from the wire oscillation [see forward flow probability (percent of the time that τ_w is in the downstream direction), or FFP, in Fig. 12] shows that the shear stress is predominantly in the downstream direction at the most upstream location and $Re_H = 4.3 \times 10^3$, in contradiction to Fig. 11. This suggests that the negative sign of the shear stress in the latter figure is resulting from the magnitude, rather than the direction conversion. This is only possible if the output voltage is outside the calibration range, suggesting that this is an erroneous point.

Table 1 Reattachment length values

Re_H	x_r/H ($C_f = 0$)	x_r/H (FFP = 50%)	Difference, %	x_r/H (mean)
4.3×10^3	4.26	4.33	1.43	4.30
8.7×10^3	4.60	4.67	1.45	4.64
13×10^3	4.84	4.88	1.00	4.86

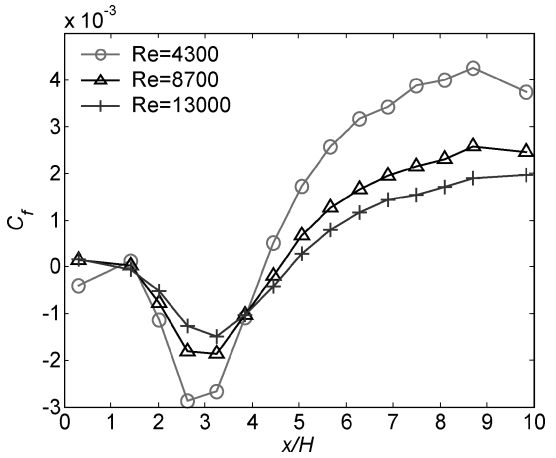

Fig. 11 Streamwise distribution of the mean skin-friction coefficient.

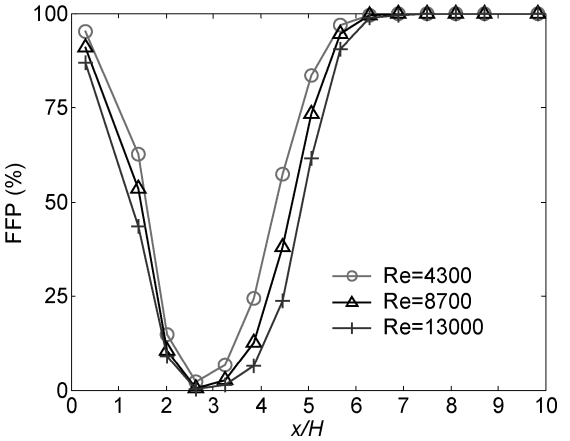

Fig. 12 Streamwise distribution of forward flow probability.

The mean skin-friction distribution in Fig. 11 displays two positions where C_f crosses zero. The first position close to the step defines the location of the mean secondary separation point or corner eddy length. The position, where $C_f = 0$ at the location farther downstream, gives the mean reattachment length. The values of x_r for the Reynolds numbers investigated are tabulated in Table 1.

Another method to find the mean reattachment point is using the distribution of forward/reverse flow probability, as demonstrated in Spazzini et al.,[4] Tihon et al.,[5] Eaton,[11] and Westphal and Johnston.[12] For example, an FFP of 100% means the flow is always towards the downstream direction. On the contrary, FFP = 0% means the flow is always towards the upstream direction. At the mean reattachment point, FFP = 50%. Figure 12 displays three curves representing the FFP distribution for all three Reynolds numbers, which exhibit the same trend. Consistent with the distribution of the mean skin-friction coefficient, there are also two positions where FFP = 50%. The farther downstream one indicates the mean reattachment location, the values for which are listed in Table 1.

As depicted in Table 1, the difference in determining the reattachment length using the C_f or FFP is less than 1.5%. The reattachment length slightly increases with rising Reynolds number over the range investigated. The same trend was also found by Spazzini et al.,[4]

where Re_H was varied from 3.5×10^2 through 16×10^3. The increase could be attributed to the variation of the boundary-layer thickness. Both Eaton and Johnston[13] and Adams and Johnston[14] found that the reattachment length increased slightly with decreasing boundary-layer thickness. Because the Reynolds number is increased by increasing the freestream velocity in the present study, the thickness of the boundary layer at separation does in fact decrease with increasing Reynolds number.

Another important observation is that the reattachment length x_r/H reported here is smaller than that in the bulk of the literature, for example, $x_r/H = 6.00$ at $Re_H = 5 \times 10^3$ (Jovic and Driver[3]), 5.39 at $Re_H = 5.1 \times 10^3$ (Spazzini et al.[4]), 5.1 at $Re_H = 4.8 \times 10^3$ (Tihon et al.[5]), and also smaller than the minimum x_r $(4.9H)$ reported in the review by Eaton and Johnston.[13] But in all of these studies, either a two-dimensional planar BFS geometry or sudden expansion of a pipe was used. Although the flow in the sudden expansion is also axisymmetric, the geometry has concave curvature, and the boundary-layer characteristics at separation can be different. Therefore, it is possible that the shorter reattachment length found here is caused by the geometry difference. Kim et al.[15] also found that the reattachment length in laminar boundary-layer separation over an axisymmetric BFS, composed of an elliptic-cone-shaped obstruction placed in front of a cylinder tube, was always shorter than that of the planar BFS flow. They attributed this phenomenon to the effect of transverse convex curvature.

To examine the reasonableness of this hypothesis further, the reattachment mechanism needs to be scrutinized. As argued by Eaton[11] and Adams and Johnston,[14] the reattachment physics could be attributed to the mass balance between the fluid reentrained into the shear layer and the pressure-driven backflow. For example, if there is more pressure-driven backflow, the reattachment length will increase so that the shear layer has a longer length to entrain the backflow, and the pressure gradient decreases leading to a reduction in the backflow. On the contrary, increasing entrainment rate to the shear layer will decrease the reattachment length, which has been verified in the control experiments of the backward-facing step flow, for example, Chun and Sung[16] and Lai et al.[17]

It is conjectured here that because of the axisymmetric geometry of the BFS the vortical structures at separation are substantially more coherent in the transverse (azimtuthal) direction than in the planar geometry and more capable of sustaining higher entrainment rates than in the planar geometry, leading to a shorter reattachment length. In the planar geometry, the transverse coherence, or two dimensionality, of the vortices is influenced by sidewall effects directly, as well as indirectly, through the imperfect two dimensionality of the mean flow itself. The coherence (and energy) of the vortices can be enhanced through artificial excitation of the flow. Chun and Sung[16] employed local forcing to control the turbulent flow separating over a planar BFS. The reattachment length was reduced from $7.8H$ to $5.0H$. It was shown that the forcing enhanced the shear-layer growth rate and produced roll up of a large vortex at separation, leading to higher entrainment rate and shorter reattachment length. In a similar manner, one could imagine a highly coherent vortex ring shedding from the transverse convex curvature at the step and growing quickly to a large size through pairing interactions, affecting a higher entrainment rate.

Another factor to consider in examining x_r results is the ratio of the boundary-layer thickness δ just upstream of the step to step height. In the current study at $Re_H = 13 \times 10^3$, Re_θ (Reynolds number based on boundary-layer momentum thickness) $= 2.739 \times 10^3$, $\delta/H = 1.72$, and $x_r/H = 4.88$. This can be compared with two well-documented experiments in a planar BFS flow: $Re_H = 39.455 \times 10^3$, $Re_\theta = 852$, $\delta/H = 0.23$, and $x_r/H = 7.95$ for Eaton,[11] and $Re_H = 33 \times 10^3$, $Re_\theta = 1.340 \times 10^3$, $\delta/H = 0.41$, and $x_r/H = 7.8$ for Chun and Sung.[16] The boundary layer in all studies is turbulent. The current δ/H is the biggest, so that the reattachment should be the smallest.

B. Mean/rms Skin-Friction Coefficient and FFP

The mean skin-friction coefficient distribution is replotted in Fig. 13 after normalization of x using x_r. Data from the literature are also added to the figure for the purpose of comparison. The mean skin-friction plots in Fig. 13 are divided into two parts: for $Re_H < 10^3$ (Fig. 13a) and for $Re_H > 10^3$ (Fig. 13b), in order to show the data points clearly. Despite differences in the experiments, such as geometry and Reynolds number, all data sets exhibit the same trend. From the separation point to $x/x_r \approx 0.33$, the value of the mean skin friction is very small and slightly above zero. This region is referred to as the secondary recirculation zone, or corner eddy. Kim et al.[15] studied the axisymmetric separation and reattachment of a laminar boundary layer and were able to identify the corner eddy only when the diameter ratio of the up and downstream cylinders at the step was less than 2.0. In the current study, the diameter ratio is 1.25, and hence the finding of the corner eddy here is consistent with the conclusions of Kim et al.[15]

From $x/x_r \approx 0.33$ to 1.0, that is, within the primary recirculation region, the mean C_f is negative, and the maximum "reverse" C_f is at $x/x_r \approx 0.68$. Downstream of the reattachment, the mean C_f rises slowly to a steady value at $x/x_r \approx 2$. The magnitude of mean C_f in Tihon et al.[5] is generally higher than all other measurements. Hence, these data are not used for comparisons concerning C_f magnitude. The data at $Re_H = 13 \times 10^3$ agree well with those at $Re_H = 10.4 \times 10^3$ (Jovic and Driver[3]) and $Re_H = 10^3$ (Spazzini et al.[4]) except for the region around the maximum negative shear, where the present data are closer to those from Spazzini et al.[4] than the others. Similarly, the data at $Re_H = 8.7 \times 10^3$ collapse on those at $Re_H = 6.8 \times 10^3$ (Jovic and Driver[3]) and $Re_H = 5.1 \times 10^3$ (Spazzini et al.[4]) except for the region around the maximum shear reversal $(x/x_r = 0.68)$. The magnitude of C_f from the current data is somewhat smaller than that obtained from the other studies around $x/x_r = 0.68$.

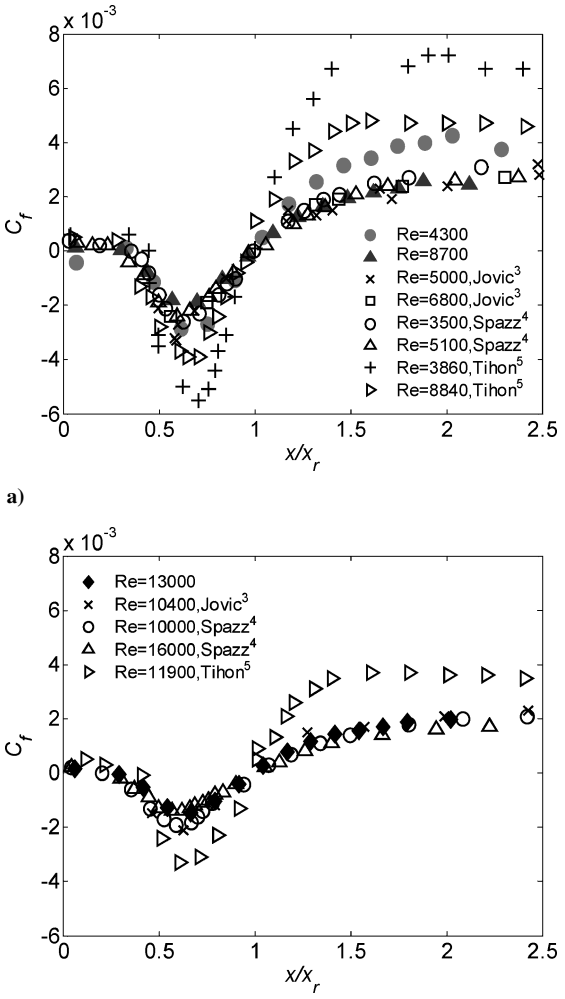

Fig. 13 Comparison of the mean skin-friction coefficient results with other studies: a) $Re_H < 10^3$ and b) $Re_H > 10^3$.

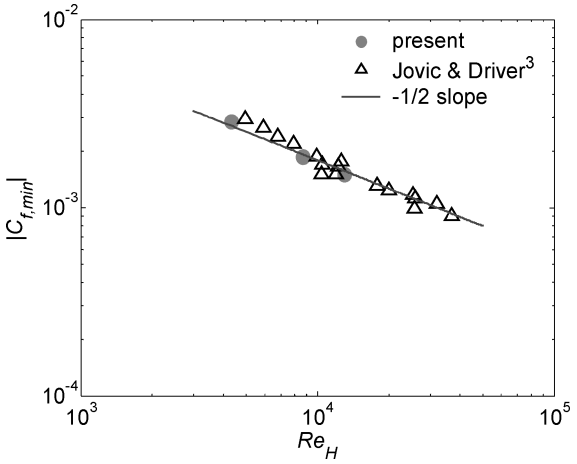

Fig. 14 Minimum skin-friction coefficient vs Re_H.

Finally, at the lowest Reynolds number of $Re_H = 4.3 \times 10^3$, the results are consistent with $Re_H = 3.5 \times 10^3$ data (Spazzini et al.[4]) upstream of reattachment. However, farther downstream, the data at $Re_H = 4.3 \times 10^3$ are obviously larger than those at $Re_H = 3.5 \times 10^3$ (Spazzini et al.[4]). The discrepancy might be caused by the differences in the geometry and/or the separating boundary-layer state. In Spazzini et al.,[4] the step has planar geometry, and the flow upstream of the point of separation is a two-dimensional fully developed channel flow.

Figure 14 depicts the magnitude of the minimum skin-friction coefficient $C_{f,\min}$, which is the maximum skin-friction coefficient of the backflow, against the Reynolds number. More data points from Jovic and Driver[3] are included in the figure for the purpose of comparison. All data points collapse fairly well onto a straight line with $-\frac{1}{2}$ slope when plotted using logarithmic scale. This kind of power-law relationship between $C_{f,\min}$ and Re_H was also found in Tihon et al.,[5] who included data from Westphal et al.,[1] Devenport and Sutton,[2] and Jovic and Driver.[3] They concluded that the flow near the wall in the primary recirculation region is viscous dominated or laminar like, where the local skin-friction coefficient is inversely proportional to square root of the Reynolds number.

Despite differences in various experiments, a universal empirical correlation between $C_{f,\min}$ and the Reynolds number provides a fairly good agreement with all data sets. Jovic and Driver[3] studied the airflow over a two-dimensional BFS geometry, Tihon et al.[5] investigated the skin-friction coefficient inside a water channel using a two-dimensional BFS geometry, whereas the current study is concerned with the airflow over an axisymmetric backward-facing step.

Figure 15 shows a comparison with published results for the forward flow probability. All of the measurements show an FFP value that is close to 100% just downstream of the step. This value decreases rapidly to 50% at $x/x_r \approx 0.33$, which marks the boundary between the corner eddy and primary recirculation region. Downstream of this position, the FFP decreases to 0% followed by an increase to 50% again at $x/x_r \approx 1$, or the reattachment position. The FFP continues to rise until it reaches 100% around $x/x_r \approx 1.33$. The x/x_r location corresponding to 50% FFP at the point separating the primary and secondary recirculation zones becomes smaller with increasing Reynolds number. This suggests that the size of the secondary recirculation zone becomes smaller relative to the primary recirculation zone as the Reynolds number increases.

The observations from Figs. 13 and 15 are quite consistent. Positive values of the mean skin-friction coefficient correspond to FFP > 50% (i.e., most of the time the flow is in the downstream direction), while negative C_f is found at locations where FFP < 50%. At FFP = 50%, $C_f \approx 0$, thus, the consistent agreement found earlier in determining x_r from FFP and C_f (see Table 1). Finally, the location of the maximum reverse shear ($x/x_r \approx 0.68$) is different from the location of FFP ≈ 0 ($x/x_r = 0.57$).

Figure 16 displays the rms skin-friction coefficient from the current measurements and those from the selected studies. The trend

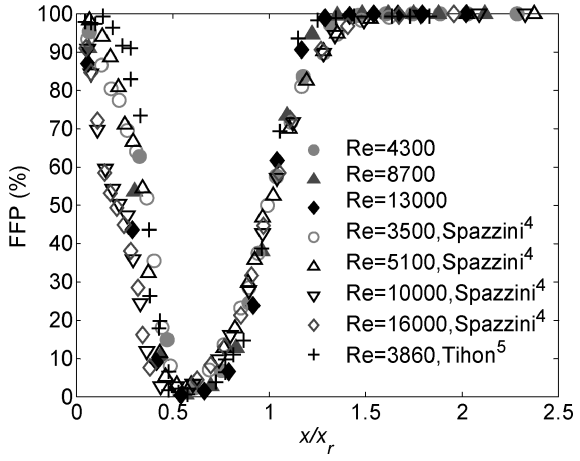

Fig. 15 Comparison of forward flow probability results with other studies.

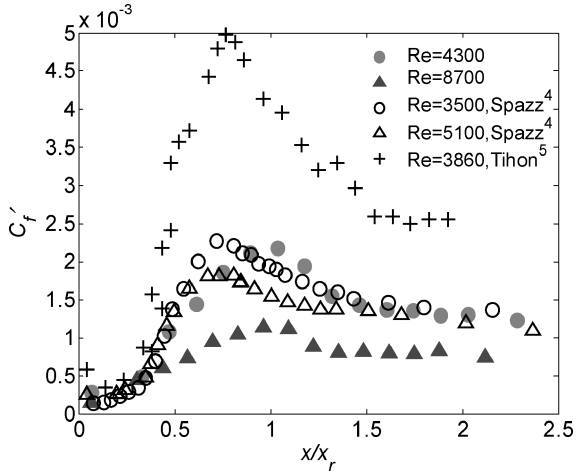

a)

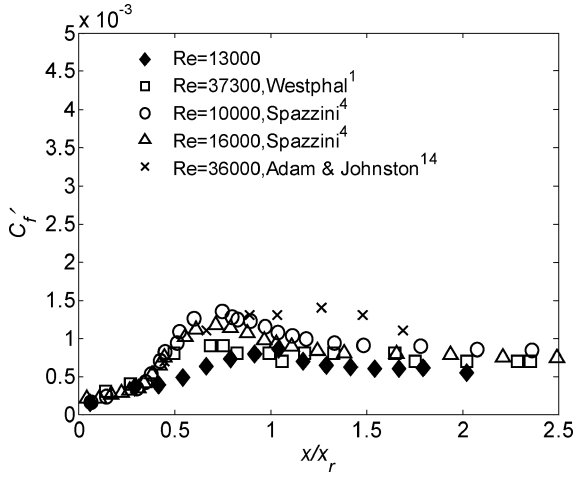

b)

Fig. 16 Comparison of rms skin-friction coefficient results with other studies: a) $Re_H < 10^3$ and b) $Re_H > 10^3$.

of C_f' is the same for all measurements. It increases monotonically with increasing x, reaching a maximum in the vicinity of the mean reattachment point, followed by a slow decay thereafter. Qualitatively speaking, the C_f' results bear similarity to those associated with the rms wall-pressure fluctuation in Lee and Sung[18] and Hudy et al.,[19] where the rms pressure rises with increasing downstream distance till $x/x_r \approx 1$ and continues to decay afterward.

This suggests that the driving mechanism of wall-shear fluctuations is linked to that of wall-pressure fluctuations. Such a link

would be consistent with the conclusions of Devenport and Sutton[2] that the fluctuations of the streamwise velocity near the wall are driven by pressure gradient fluctuations imposed by the separated shear layer. One component of this pressure gradient is that associated with the low-frequency flapping of the shear layer. The other is that generated by the momentary passage of the vortical structures above the point of τ_w observation.

The detailed characteristics of the shear-layer vortices were examined recently by Kostas et al.[20] using particle-image-velocimetry (PIV) measurements within the separated flow region. They also proposed that small-scale vortical structures were responsible for Reynolds stress and turbulent kinetic energy upstream of reattachment while large-scale structures were dominant downstream of reattachment. Moreover, Scarano et al.[21] found that the vortex formation started from $x/x_r \approx 0.17$ and that the vortices approached the bottom wall at $x/x_r \approx 0.58$ in their PIV investigation of a BFS flow. Owing to their smaller size and larger distance above the wall, the smaller vortices found near separation presumably have less of an effect on the wall shear than the larger ones, farther downstream. The gradual increase in C'_f with x/x_r is, thus, partly a manifestation of the increase in energy of the passing vortices and their movement closer to the wall.

Near the step, the very small skin-friction fluctuation could be caused by the unsteadiness of the corner eddy, which is associated with the flapping of the shear layer. Downstream of the reattachment, C'_f decays slowly because of the lack of free shear-layer activity there. The energized vortical structures from the separated shear layer decay and diffuse as they travel downstream.

Comparing the magnitude of C'_f from the vaious investigations, the data from Tihon et al.[5] are higher than others, as was the case with the mean C_f results (see Fig. 13). Although the data from Westphal et al.[1] and Adam and Johnston[14] are close to those from Spazzini et al.,[4] they were obtained at a much higher Reynolds number. Except near x_r, the current rms skin-friction coefficient values at $Re_H = 4.3 \times 10^3$ fall between the data at $Re_H = 3.5 \times 10^3$ and 5.1×10^3 from Spazzini et al.[4] At $Re_H = 8.7 \times 10^3$ and 13×10^3, the current data are smaller than that at $Re_H = 10 \times 10^3$ and $Re_H = 16 \times 10^3$, respectively. However, the reader is reminded of the axisymmetric geometry of the backstep used here, which might be the cause of some of the observed differences. Additionally, with the exception of the data from Tihon et al.,[5] all other investigations employed one or more variation of thermal-wake tagging by a heated wire to detect the flow direction. The present investigation is the first to employ flow direction detection that is not based on thermal-wake detection.

It is also interesting to examine the location of the peak rms skin-friction coefficient. The data from Westphal et al.[1] and Spazzini et al.[4] peak at $x/x_r \approx 0.72$, Tihon et al.[5] at $x/x_r \approx 0.76$, Adam and Johnston[14] at $x/x_r \approx 1.25$, whereas the current results exhibit the peak at $x/x_r = 1$. It is well documented that the peak rms wall pressure occurs slightly upstream of the reattachment point in two-dimensional BFS and splitter plate. Lee and Sung[18] found the peak rms wall pressure at 0.93, Hudy et al.[19] at 0.92, Driver et al.[22] at $x/x_r \approx 0.91$, and Heenan and Morrsion[23] at 0.91. Because of the limited number of measurement locations, there are no sensor data available from $x/x_r = 0.9$–1.0 in the current study. It is possible that the maximum rms skin-friction coefficient found here could be located at $x/x_r = 0.9$–1.0, which would be consistent with the wall-pressure measurements.

C. Power Spectrum Results

The power spectra of the fluctuating wall-shear stress τ'_w at different locations are plotted in Fig. 17 for Reynolds numbers of 8.7×10^3. To avoid clutter of the plot, each spectrum was shifted up by one decade relative to that obtained one x location upstream of it. The spectra magnitudes and frequency f are normalized using the dynamic head and the reattachment length/freestream velocity, respectively. The resulting nondimensional quantities are denoted using an asterisk superscript.

Two primary observations can be made from Fig. 17. First, the spectrum value decays with increasing frequency at all x locations.

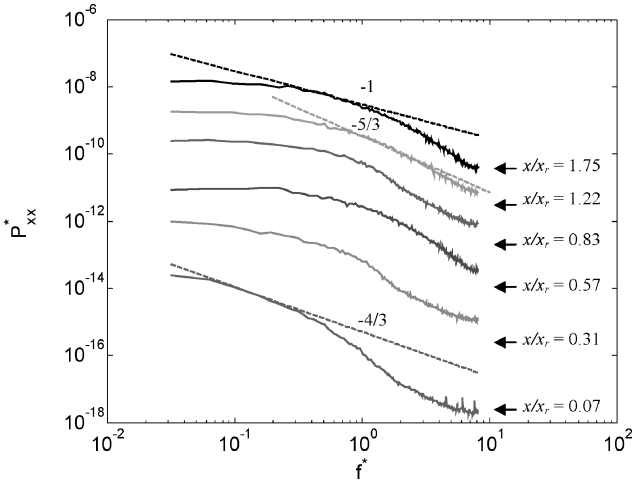

Fig. 17 Wall-shear power spectra at different x locations for $Re_H = 8.7 \times 10^3$.

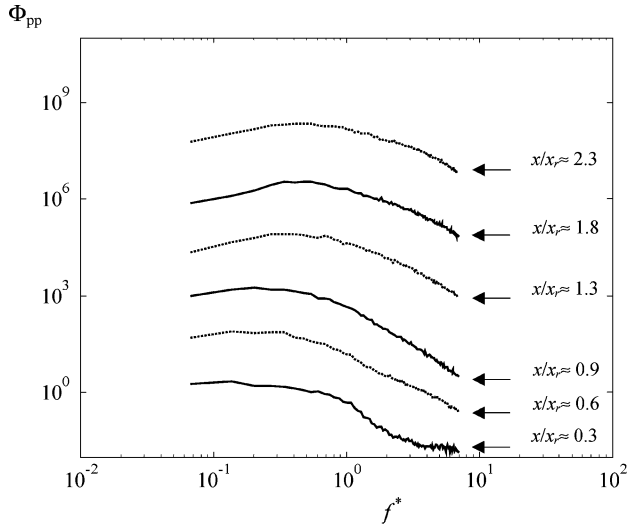

Fig. 18 Power spectra of the fluctuating wall pressure at different x locations and $Re_H = 8.7 \times 10^3$ (Hudy, private communication, 2003).

This is fundamentally different from wall-pressure spectra, which exhibit a spectrum peak switch with increasing x. To demonstrate, wall-pressure spectra measured by L. M. Hudy (private communication, Michigan State University, East Lansing, Michigan, Nov. 2003) on the same model and at the same Reynolds number of $Re_H = 8.7 \times 10^3$ are shown in Fig. 18. Unlike τ'_w spectra, the peak of the wall-pressure spectrum switches from being within the low-frequency range near separation to a frequency of $f^* \approx 0.5$ for $x/x_r > 0.9$.

Although no τ'_w spectrum peak is found around $f^* \approx 0.5$ in Fig. 17, there is a clear "filling" of the spectrum in the vicinity of this frequency as x increases. This can be identified by the decrease in the spectrum slope in the middle range of frequencies as identified in the figure. For x approximately less than $0.3x_r$, a slope of $-\frac{4}{3}$ is found. At larger x locations, the slope becomes -1. Also at locations sufficiently far downstream $x/x_r > 0.8$, the spectral slope at the high-frequency end exhibits a $-\frac{5}{3}$ slope. This is indicative of the establishment of an inertial subrange, presumably associated with the redevelopment of the boundary layer after reattachment.

The rise in the spectrum energy in the middle range of frequencies (around $f^* \approx 0.5$) as x approaches x_r can be seen more clearly by plotting the spectra on a semilog plot, as seen in Fig. 19. For these plots, the horizontal axis is $\log(f^*)$, and the vertical axis is linear and represents the product of $P^*_{xx} \times f^*$. In this fashion, the geometrical area under the spectra represents the energy level. For example, the area under the spectra around $x/x_r = 0.06$ is smallest, which corresponds to very small energy, that is, very small fluctuation of τ_w.

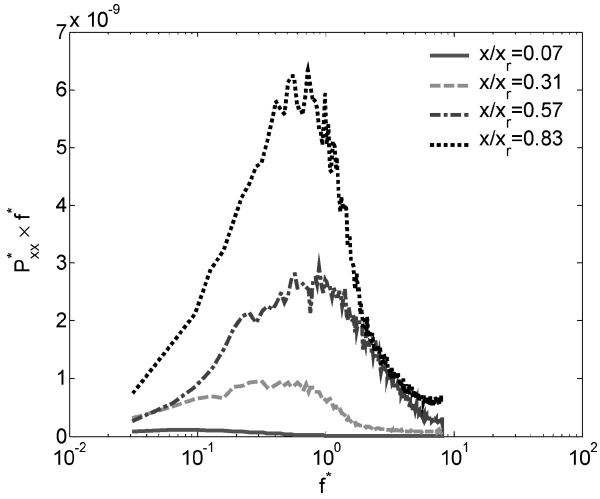

Fig. 19 Wall-shear power spectra plotted on semilog scale for different x locations and $Re_H = 8.7 \times 10^3$.

On the contrary, the area under the spectra around the reattachment position is largest, where the fluctuation is highest.

At $x/x_r = 0.06$, most contributions to the total energy come from low frequencies for all three Reynolds numbers. The energy content is concentrated around a frequency of $f^* \approx 0.1$. Spazzini et al.[4] also detected a peak at $f^* \approx 0.08$ in the wall-shear spectra measured upstream of $0.28x_r$. A peak at $f^* \approx 0.16$ was found in the pressure measurements of Hudy et al.[19] upstream of $0.25x_r$. For the locations downstream of $x/x_r \approx 0.30$, the buildup of energy up to the reattachment location clearly falls in a frequency range that is centered around an f^* value 0.65 (Fig. 19). This frequency range encompasses the passage frequency of the shear-layer vortices, as reported in the literature. Thus, it is apparent that the increased level of wall-shear fluctuations is a manifestation of the increased energy and proximity of these vortices as they approach the reattachment point.

The two frequencies of $f^* = 0.1$ and 0.65 were also identified in the limited wall-shear literature available. For example, Spazzini et al.[4] found the low and high frequencies to be $f^* = 0.08$ and 1.0, respectively. More abundant observations of these frequencies are available from wall-pressure measurements. Peak frequencies of $f^* = 0.11$ and 0.50 were found by Lee and Sung[18] in BFS flow, $f^* = 0.12$–0.18 and 0.6–0.9 by Hudy et al.[19] in a fence/splitter-plate model, and $f^* = 0.18$ and 0.6 by Driver et al.[22] in BFS flow.

V. Summary

A high-frequency oscillating-hot-wire (OHW) sensing technique for measurement of the flow-velocity/wall-shear-stress magnitude and direction was developed for the first time in the current work. The calibration and characterization of the OHW sensor were conducted in a Couette flow facility. The new sensor, oscillating at a frequency of 2.8 kHz, was used to investigate the wall-shear signature beneath an axisymmetric BFS flow at different streamwise locations downstream of the step.

The mean reattachment length is found to be smaller than those reported in the literature for planar BFS flows. It is hypothesized that the reduction in the reattachment length is caused by enhanced entrainment of the separated shear layer in the axisymmetric case and/or transverse curvature of the test model. The distribution of mean and rms skin-friction coefficient is consistent with the wall-shear literature. The power spectra of fluctuating wall shear reveal two characteristic frequencies: shear-stress unsteadiness with $f^* \approx 0.1$ was found to be dominant very close to the step; and wall-shear fluctuation with $f^* \approx 0.65$ dominated farther downstream positions. Comparison of wall-pressure and wall-shear spectra shows some difference. In wall-pressure spectra, the spectral peak switches from the lower frequency corresponding to shear-layer flapping to the higher frequency associated with vortex passage as x increases beyond the reattachment location. This peak switching was not observed in wall-shear spectra.

Acknowledgment

This work is supported by Grant CTS-0116907 from the National Science Foundation.

References

[1]Westphal, R. V., Eaton, J. K., Johnston, J. P., "A New Probe for Measurement of Velocity and Wall Shear Stress in Unsteady Reversing Flows," *Journal of Fluids Engineering*, Vol. 103, Sept. 1981, pp. 478–482.

[2]Devenport, W. J., and Sutton, E. P., "Near-Wall Behavior of Separated and Reattaching Flows," *AIAA Journal*, Vol. 29, No. 1, 1991, pp. 25–31.

[3]Jovic, S., and Driver, D., "Reynolds Number Effect on the Skin Friction in Separated Flows Behind a Backward-Facing Step," *Experiments in Fluids*, Vol. 18, No. 6, 1995, pp. 464–467.

[4]Spazzini, P. G., Iuso, G., Onorato, M., Zurlo, N., and Cicca, G. M. D., "Unsteady Behavior of Back-Facing Step Flow," *Experiments in Fluids*, Vol. 30, No. 5, 2001, pp. 551–561.

[5]Tihon, J., Legrand, J., and Legentilhomme, P., "Near-Wall Investigation of Backward-Facing Step Flows," *Experiments in Fluids*, Vol. 31, No. 5, 2001, pp. 484–493.

[6]Naughton, J. W., and Sheplak, M., "Modern Developments in Shear-Stress Measurement," *Progress in Aerospace Sciences*, Vol. 38, No. 6–7, 2002, pp. 515–570.

[7]Fernholz, H. H., Janke, G., Schober, M., Wagner, P. M., and Warnack, D., "New Developments and Applications of Skin-Friction Measuring Techniques," *Measurement Science and Technology*, Vol. 7, No. 10, 1996, pp. 1396–1409.

[8]Li, Y., and Naguib, A. M., "An Oscillating Hot-Wire Technique for Resolving the Magnitude and Direction of Velocity Measurements Using Single Hot-Wire Sensors," *Experiments in Fluids*, Vol. 34, No. 5, 2003, pp. 597–606.

[9]Elger, D. F., and Adams, R. L., "Dynamic Hot-Wire Anemometer Calibration Using an Oscillating Flow," *Journal of Physics E: Scientific Instruments*, Vol. 22, No. 3, 1989, pp. 166–172.

[10]Khoo, B. C., Chew, Y. T., and Lim, C. P., "The Flow Between a Rotating and a Stationary Disc: Application to Near-Wall Hot-Wire Calibration," *Measurement Science and Technology*, Vol. 9, No. 4, 1998, pp. 650–658.

[11]Eaton, J. K., "Turbulent Flow Reattachment: an Experimental Study of the Flow and Structure Behind a Backward-Facing Step," Ph.D. Dissertation, Dept. of Mechanical Engineering, Stanford Univ., Stanford, CA, 1980.

[12]Westphal, R. V., and Johnston, J. P., "Effect of Initial Conditions on Turbulent Reattachment Downstream of a Backward-Facing Step," *AIAA Journal*, Vol. 22, No. 12, 1984, pp. 1727–1732.

[13]Eaton, J. K., and Johnston, J. P., "A Review of Research on Subsonic Turbulent Flow Reattachment," *AIAA Journal*, Vol. 19, No. 9, 1981, pp. 1093–1099.

[14]Adams, E. W., and Johnston, J. P., "Effects of the Separating Shear Layer on the Reattachment Flow Structure Part 2: Reattachment Length and Wall Shear Stress," *Experiments in Fluids*, Vol. 6, No. 7, 1988, pp. 493–499.

[15]Kim, K. C., Yang, J. P., and Boo, J. S., "An Experimental Study on the Structure of a Turbulent Reattaching Flow Behind an Axisymmetric Backward-Facing Step," Fluids Engineering Div., FED Vol. 237, No. 2, American Society of Mechanical Engineers, New York, 1996, pp. 863–870.

[16]Chun, K. B., and Sung, H. J., "Control of Turbulent Separated Flow over a Backward-Facing Step by Local Forcing," *Experiments in Fluids*, Vol. 21, No. 6, 1996, pp. 417–426.

[17]Lai, J. S. C., Yue, J., and Platzer, M. F., "Control of Backward-Facing Step Flow Using a Flapping Foil," *Experiments in Fluids*, Vol. 33, No. 1, 2002, pp. 44–54.

[18]Lee, I., and Sung, H. J., "Characteristic of Wall Pressure Fluctuations in Separated Flows over a Backward-Facing Step: Part I. Time-Mean Statistics and Cross-Spectral Analysis," *Experiments in Fluids*, Vol. 30, No. 3, 2001, pp. 262–272.

[19]Hudy, L. M., Naguib, A. M., and Humphreys, W. M., "Wall-Pressure-Array Measurements Beneath a Separating/Reattaching Flow Region," *Physics of Fluids*, Vol. 15, No. 3, 2003, pp. 706–717.

[20]Kostas, J., Soria, J., and Chong, M. S., "Particle Image Velocimetry Measurements of a Backward-Facing Step Flow," *Experiments in Fluids*, Vol. 33, No. 6, 2002, pp. 838–853.

[21]Scarano, F., Benocci, C., and Riethmuller, M. L., "Pattern Recognition Analysis of the Turbulent Flow past a Backward Facing Step," *Physics of Fluids*, Vol. 11, No. 12, 1999, pp. 3808–3818.

[22]Driver, D. M., Seegmiller, H. L., and Marvin, J. G., "Time-Dependent Behavior of a Reattaching Shear Layer," *AIAA Journal*, Vol. 25, No. 7, 1987, pp. 914–919.

[23]Heenan, A. F., and Morrison, J. F., "Passive Control of Pressure Fluctuations Generated by Separated Flow," *AIAA Journal*, Vol. 36, No. 6, 1998, pp. 1014–1022.

J. Trolinger
Guest Editor